Formation of a two-dimensional layered structure in silica under shear stresses: An *ab initio* study

Murat Durandurdu
Department of Physics, University of Texas at El Paso, El Paso, Texas 79968, USA
and Fizik Bölümü, Ahi Evran Üniversitesi, Kırşehir 40100, Turkey
(Received 20 July 2009; revised manuscript received 31 January 2010; published 10 May 2010)

The behavior of α-cristobalite under pure shear stresses is studied using an *ab initio* technique. The application of shear stress on the *a*-*b* planes yields a two-dimensional layered monoclinic phase with C_2 space group via an orthorhombic phase having $C222_1$ symmetry. In the layered structure, each silicon atom is fourfold coordinated. On the other hand, shearing of *a*-*c* and *b*-*c* planes causes first a transformation into monoclinic phases within $P2_1$ symmetry and then structural failure. We also study the behavior of α-cristobalite under the simultaneous application of shear stress and hydrostatic pressure. We consider six different loading conditions and find that the shear stresses have no influence on the densification mechanism until a first-order phase transformation occurs. On the other hand, the shear stresses play a significant role during the first-order phase transformation and result in the *Cmcm*, anataselike, and stishovite structures in our simulations. The phase transformation from α-cristobalite to the *Cmcm* structure is due to the shear deformation on the *a*-*b* planes and proceeds via an orthorhombic intermediate phase having $C222_1$ symmetry.

DOI: 10.1103/PhysRevB.81.174107 PACS number(s): 61.50.Ks, 62.50.−p, 64.70.−p

I. INTRODUCTION

Understanding the high-pressure behavior of silica has been long interests in earth and material sciences and fundamental solid-state physics and chemistry. Silica is therefore a well-studied material. However, there are still unknowns and controversies.

Among silica polymorphs, α-cristobalite, is a tetrahedrally coordinated structure with $P4_12_12$ space-group symmetry and four SiO_2 formula units in the unit cell. The high-pressure phase of this crystal has been studied extensively and to date several high-pressure phases have been reported in experiments and simulations. Experiments showed that α-cristobalite transforms into a low symmetric monoclinic phase around 1.5 GPa.[1] Tsuchida and Yagi[2,3] observed that α-cristobalite transforms into several unknown phases labeled phase X-I, X-II, and X-III. These phase transformations were confirmed in later study[4] but attempts to index these structures had failed because of the weak and broad diffraction peaks. The structure of phase X-I was recently determined in our previous simulations and was characterized by a hexagonal close packing of the oxygen sublattice.[5] The phase X-II was identified as an α-PbO_2-like silica later.[6,7] The nature and structure of phase X-III formed upon pressure release are still unknown. In another investigation, quasihydrostatic compression of α-cristobalite[8] led to the formation of a structure similar to stishovite when exceeding 20 GPa.

The pressure-induced phase transformations of α-cristobalite also have been explored using constant-pressure simulations. Using a molecular-dynamics (MD) method with a semiempirical potential-energy function, Tsuneyuki *et al.*[9] discovered that low-cristobalite first transforms to a new silica structure type with space-group symmetry *Cmcm* with equal numbers of four- and six-coordinate Si atoms and then to the stishovite structure. Recent simulations using an empirical potential,[10] on the other hand, suggested that α-cristobalite transforms into the anataselike or stishovite phases depending on the loading rate: the low compression rate resulted in an anataselike structure while a higher compression rate yielded a much higher transition pressure and a phase transformation into stishovite. A direct transition into stishovite was observed in an *ab initio* MD simulation.[11] In our preliminary study using both a constant-pressure *ab initio* technique and classical MD simulations, we observed the α-cristobalite $\rightarrow$ phaseX-I $\rightarrow$ stishovite phase transformations.[5] The behavior of α-cristobalite under nonhydrostatic conditions was also explored using constant-pressure simulations.[10,12,13] Several phases of silica including α-PbO_2-like were predicted in these studies.

In this work, we extend our study and explore the behavior of α-cristobalite under pure shear stresses and the simultaneous application of shear stress and hydrostatic pressure. The application of pure shear stress on the *a*-*b* planes first produces an orthorhombic structure having $C222_1$ symmetry and then a transformation into a layered monoclinic phase with C_2 space group. On the other hand, monoclinic phases having $P2_1$ symmetry form when α-cristobalite is subjected to shear stress on *a*-*c* and *b*-*c* planes. For the simultaneous application of shear and hydrostatic stresses, we observe the formation of three phases, *Cmcm*, anataselike, and stishovite depending on the shear deformations.

II. METHOD

We performed first-principles calculations using the pseudopotential method within the density-functional theory (DFT) formalism and the generalized gradient approximation (GGA) of Perdew-Bucker and Ernzerhof[14] to evaluate the exchange-correlation energy. The calculations were carried out using SIESTA,[15] a DFT code that uses a linear combination of atomic orbitals as the basis set and norm-conserving Troullier-Martins pseudopotentials.[16] An optimized split-valence double-ξ plus polarized basis set was employed. A

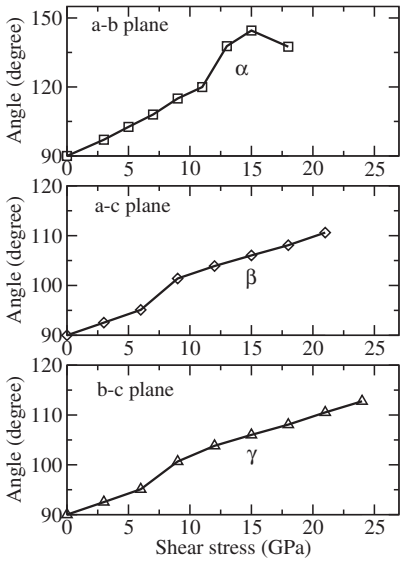

FIG. 1. The change in simulation cell angles as a function of pure shear stresses on the *a*-*b* planes (top panel), the *a*-*c* planes (middle plane), and the *b*-*c* planes (bottom panel). α is the angle between **a** and **b** vectors. β is the angle between **a** and **c** vectors. γ is the angle between **b** and **c** vectors.

uniform mesh with a plane-wave cutoff of 120 Ry was used to present the electron density, the local part of the pseudopotential, and the Hartree and the exchange-correlation potential. The simulation cell consists of 96 atoms with periodic boundary conditions. We used Γ-point sampling for the supercell's Brillouin-zone integration which is reasonable for a cell with 96 atoms. For the application of pure shear stresses, we set the shear components $\sigma_{xy}=\sigma_{yx}=P$ or $\sigma_{xz}=\sigma_{zx}=P$ or $\sigma_{yz}=\sigma_{zy}=P$ while for the application of shear and hydrostatic stresses, we set the diagonal stress components $\sigma_{xx}=P$, $\sigma_{yy}=P$, and $\sigma_{zz}=P$, and shear components $\sigma_{xy}=\sigma_{yx}=\gamma_{xy}P$, $\sigma_{xz}=\sigma_{zx}=\gamma_{xz}P$, and $\sigma_{yz}=\sigma_{zy}=\gamma_{yz}P$, where P and γ_{ij} $(i,j=x,y,z)$ are the applied external pressure and the percentage of the shear stress, respectively. The applied stress was gradually increased by an increment of 2–3 GPa for pure shear stress and of 10 GPa for the simultaneous application of shear stress and hydrostatic stresses For each value of the applied stress, the lattice vectors and the atomic positions were optimized together until the stress tolerance was less than 0.5 GPa and the maximum atomic force was smaller than 0.01 eV Å^{-1}. For minimization of geometries, a variable-cell shape conjugate-gradient method under a constant pressure was used. For the energy-volume calculations, we considered the unit cell for SiO_2 phases. In order to determine symmetry of the high-pressure phases formed in the simulations, we used the KPLOT program[17] that provides detailed information about space group, cell parameters, and atomic position of a given structure. For the symmetry analysis, we used 0.1 Å, 4°, and 0.7 Å tolerances for bond lengths, bond angles, and interplanar spacing, respectively.

III. RESULTS

A. Pure shear stresses

We apply pure shear stress on *a*-*b*, *a*-*c*, and *b*-*c* planes of α-cristobalite. In Fig. 1, we plot the change in simulation cell

TABLE I. The atomic fractional coordinates and the lattice parameters of the phases formed under pure shear stresses.

Structure	*a* (Å)	*b* (Å)	*c* (Å)	β (deg)	*x*	*y*	*z*
$P2_1$ (*a*-*c* plane)	5.05955	5.06183	7.01633	95.09	Si: 0.062395	0.303115	0.877496
(21 GPa shear stress)					Si: 0.455099	0.697757	0.373080
					O: 0.995320	0.107686	0.055008
					O: 0.516862	0.886383	0.562585
					O: 0.138884	0.738774	0.310977
					O: 0.365172	0.265142	0.808456
$P2_1$ (*b*-*c* plane)	5.05939	5.06136	7.01699	95.09	Si: 0.455006	0.697747	0.873114
(24 GPa shear stress)					Si: 0.062445	0.303081	0.377416
					O: 0.634755	0.765190	0.691598
					O: 0.861189	0.238728	0.188951
					O: 0.004537	0.607543	0.445102
					O: 0.483111	0.386285	0.937345
$C222_1$ (*a*-*b* plane)	7.60232	6.71936	7.08055		Si: 0.000000	0.308091	0.250000
(13 GPa shear stress)					Si: 0.795535	0.000000	0.000000
					O: 0.071421	0.178991	0.432046
					O: 0.831390	0.557510	0.680188
C_2 (*a*-*b* plane)	4.40410	4.01970	3.53427	98.21	Si: 0.000000	0.004874	0.500000
(15 GPa shear stress)					O: 0.229456	0.760960	0.277489
$P\bar{4}m2$	2.8551		4.5475		Si: 0.500000	0.50000	0.500000
(0 GPa stress)					O: 0.000000	0.500000	0.307785

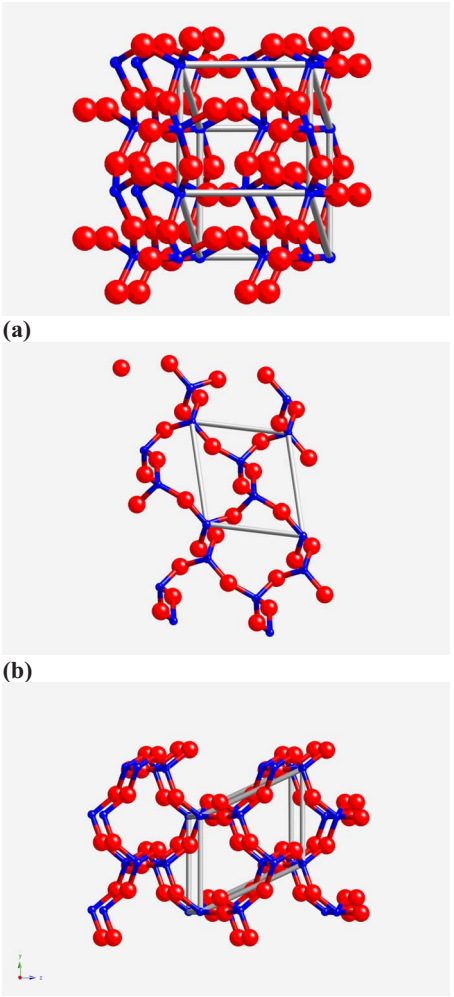

FIG. 2. (Color online) The monoclinic phase obtained under pure shear stress. Viewed along (a) [001], (b) [010], and (c) [001] directions.

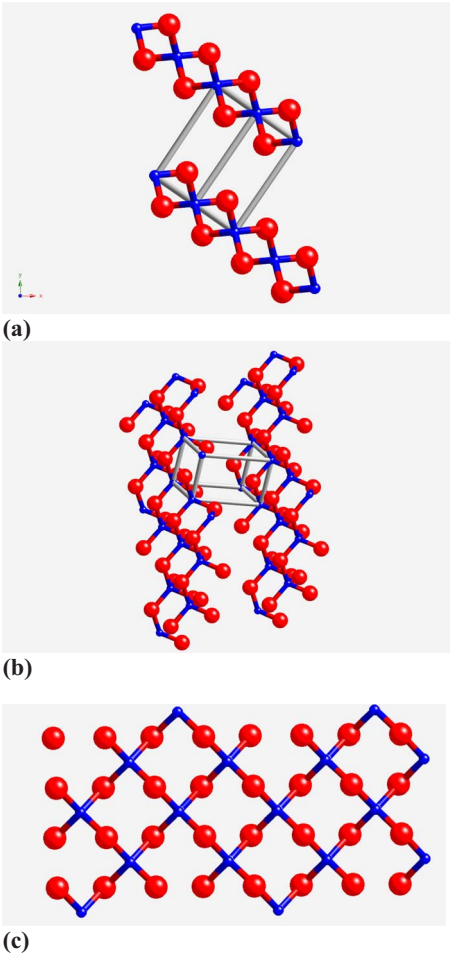

FIG. 3. (Color online) (a) and (b) Tetragonal phase and (c) single layer.

angles as a function of pure shear stresses. As expected, the shear stresses cause dramatic distortions in the structure and bond bending rather than bond compression. Therefore, the Si-O bond lengths do not vary with shear stresses. Carefully analyses reveal that the application of shear stress on *a*-*c* and *b*-*c* planes produces a monoclinic phase within $P2_1$ symmetry. This phase is shown in Fig. 2 and its atomic positions are given in Table I. The monoclinic phase is still fourfold coordinated and results from the angular distortions. Further increase in the shear stress causes structural failure at 21–24 GPa for the *a*-*c* plane shearing and 24–27 GPa for the *b*-*c* plane shearing. The $P2_1$ phase is found to be stable at zero stress with a monoclinic angle of about 91.52°. The application of shear stress on the *a*-*b* planes, on the other hand, yields an orthorhombic crystal having $C222_1$ symmetry and this symmetry is maintained up to 15 GPa at which point, a monoclinic crystal with space group C_2 is formed. The C_2 phase has a layered structure in which each Si atom is still fourfold coordinated. The Si-O bond lengths are uniform and have a value of 1.68 Å. The O-Si-O angles range from 98° to 125°. When the C_2 structure is relaxed at zero stress, a phase change into a tetragonal state within $P\bar{4}m2$ symmetry is observed. The tetragonal phase is illustrated in Fig. 3. Indeed, C_2 can be considered as a distorted $P\bar{4}m2$ phase. In the $P\bar{4}m2$ crystal, the Si-O bond lengths are about 1.67 Å and the O-Si-O angles are about 117°. Another interesting property of this phase is that both Si-Si and O-O separations in a single layer have a value of 2.85 Å. It should be noted that each layer possesses square symmetry (see Fig. 3).

The $P2_1$, $C222_1$, and $P\bar{4}m2$ phase transformations are a displacive-type transformation and are due to the angular distortions whereas the $C222_1$-to-C_2 phase transformation is a reconstructive phase transformation and requires bond breaking and formation of new bonds as shown in Fig. 4.

Perhaps, the most remarkable observation so far is the formation of a layered phase in silica. Is this phase energetically favorable relative to the other phases of silica? In order to answer this question, we calculate the energy of some of SiO_2 phases (*Cmcm*, stishovite, anatase, and α-cristobalite) at zero pressure and plot the data in Fig. 5. As can be seen from the figure, the energy of $P\bar{4}m2$ phase is larger than that of other phases except the *Cmcm* phase but comparing the energetic of the $P\bar{4}m2$ phase with that of the other phases of SiO_2, we see that the energetic of the $P\bar{4}m2$ crystal is also

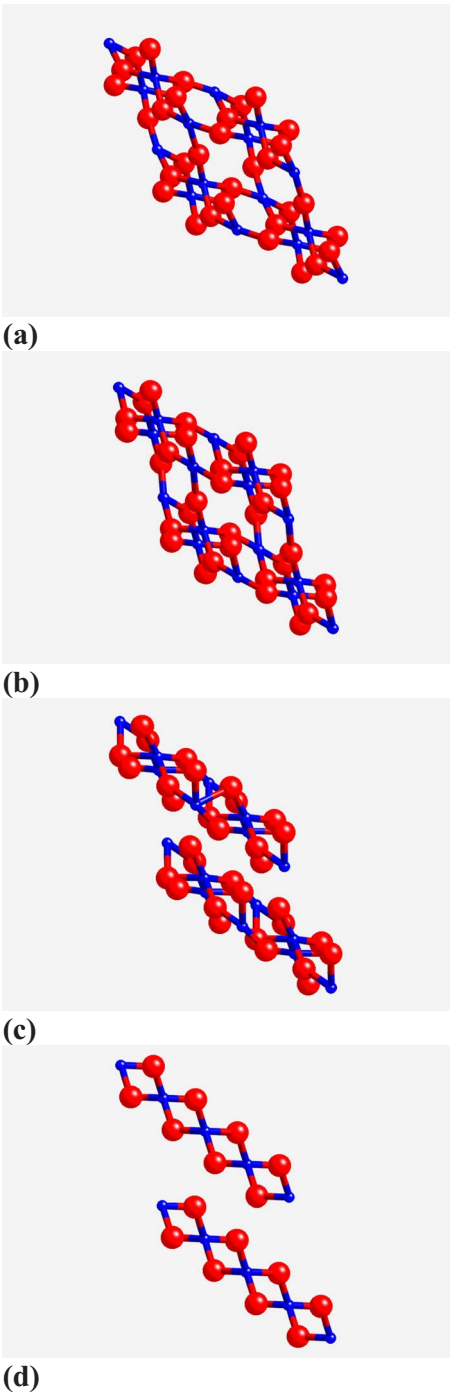

FIG. 4. (Color online) Evolution of layerlike phase (C_2) at 15 GPa.

favorable. The C_2 and $P\bar{4}m2$ phases of SiO_2 might offer several applications in technology, in particular, in the development of SiO_2-based nanomaterials, i.e., nanotubes and nanocages. Indeed, in some previous first-principles studies,[18,19] SiO_2 sheets, similar to what has been observed in the present study, were considered to model SiO_2 nanotubes or nanocages but the synthesizing of this phase with the application of pure shear stress is probably a challenging task for experimentalists because there is no experimental technique to apply pure shear stress, to our knowledge. Yet, a

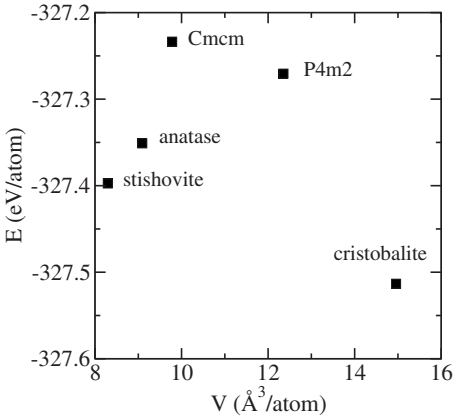

FIG. 5. Energy of silica phases.

single SiO_2 layer might be experimentally produced as a thin film. Recent studies show that the ultrathin silica film consists of a two-dimensional network of corner-sharing SiO_4 tetrahedra chemisorbed on the unreconstructed Mo(112) surface.[20–23] The structure of the films is based on a two-dimensional hexagonal layer. Furthermore, the formation of one-dimensional silica structures (stripes) on the Mo(112) surface has been observed at low Si coverage.[24] All these studies clearly demonstrate that unexpected variety of low-dimensional silica phases can be synthesized under different conditions. Based on these observations, one might expect that the layered structure observed in the present study can be also produced experimentally as an ultrathin film. Note that the single layer has a square symmetry with a 2.85 Å lattice parameter and hence it can be growth on a cubic substrate having about 2.85 Å lattice constant.

In order to determine the bulk properties of the $P\bar{4}m2$ structure, we study its energy as a function of volume using the variable-cell optimization technique and fit the energy-volume data to the third-order Birch-Murnaghan equation of state. We should note here that the layer-layer separation dramatically increases in the tensile regime, indicating weak

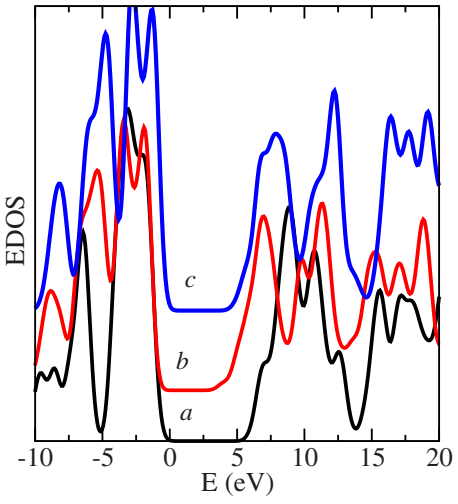

FIG. 6. (Color online) The EDOS near the band-gap region for (a) α-cristobalite, (b) tetragonal ($P\bar{4}m2$), and (c) single-layer structures.

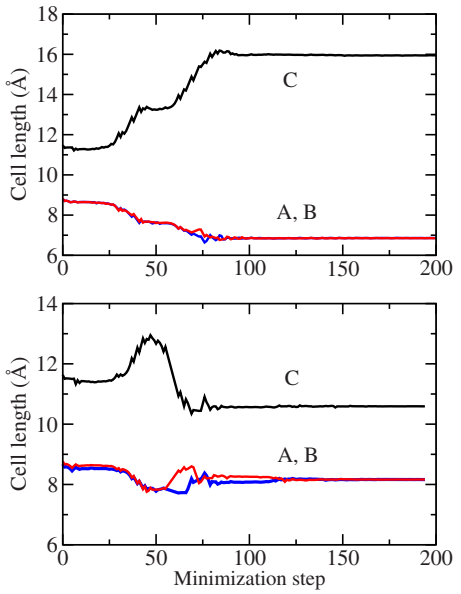

FIG. 7. (Color online) The modification of simulation cell lengths as a function of minimization step during the evolution of the anataselike (top) and stishovite (bottom) phases.

forces between the layers. This phase shows structural failure and below −1.0 GPa. From the energy-volume data, the bulk modules of $P\bar{4}m2$ is calculated to be 14.65 GPa, which is close to that of α-cristobalite, 12.52 GPa predicted in the present study.

In order to study the electronic structure of the $P\bar{4}m2$ phase and single layer,[25] we calculate their electron density of states (EDOS) and present our results in Fig. 6. The band-gap α-cristobalite is calculated to be 5.47 eV, in good agreement with the previous DFT results of 5.58 and 5.52 eV.[26,27] The band-gap energy of the $P\bar{4}m2$ phase and the single layer is predicted to be 3.54 eV and 4.38 eV, respectively. These values are noticeably smaller than that of α-cristobalite. It should be noted that the band gaps obtained from the present calculation is incomparable to experimental results because of the well-known shortcoming of DFT within the GGA in describing excited states. Nevertheless, these types of calculation give an idea about the electronic structure of the $P\bar{4}m2$ and single layer relative to that of α-cristobalite.

B. Simultaneous application of shear and hydrostatic stresses

We study six different simultaneous applications of shear stress and hydrostatic pressure to probe the influence of shear stress on the structural phase transformation of α-cristobalite and summarize our results in Table II. As seen from Table II, we observe the formation of the stishovite, *Cmcm*, and anataselike structures owing to the first-order phase transformation. In stishovite, each SiO_6 octahedra shares corners with eight neighbors, and shares edges with two other neighbors, forming a linear chain. On the other hand, in anatase, each SiO_6 octahedra shares corners with four neighbors, and shares edges with four other neighbors, forming a zigzag chain with a screw axis. The *Cmcm* structure has equal numbers of fourfold- and sixfold-coordinated Si atoms.

TABLE II. The structure observed under the simultaneous application of shear stress and hydrostatic pressure. The shear-stress components $\sigma_{xy}=\sigma_{yx}=\gamma_{xy}P$, $\sigma_{xz}=\sigma_{zx}=\gamma_{xz}P$, and $\sigma_{yz}=\sigma_{zy}=\gamma_{yz}P$, where P and $\gamma_{ii=xy,xz,yz}$ are the applied external pressure and the percentage of the shear stress, respectively.

γ_{xy}	γ_{xz}	γ_{yz}	Gradual phase transformation	First-order phase transformation
0	0	0.0	Tetragonal $P4_12_12$	Stishovite $P42/mnm$ (40 GPa)
0.05	0	0	Tetragonal $P4_12_12$	Orthorhombic *Cmcm* (30 GPa)
0	0.05	0	Tetragonal $P4_12_12$	Anatase $I4_1/amd$ (40 GPa)
0	0	0.05	Tetragonal $P4_12_12$	Stishovite $P42/mnm$ (40 GPa)
0.05	0.05	0	Tetragonal $P4_12_12$	Orthorhombic *Cmcm* (30 GPa)
0.05	0	0.05	Tetragonal $P4_12_12$	Orthorhombic *Cmcm* (30 GPa)
0	0.05	0.05	Tetragonal $P4_12_12$	Stishovite $P42/mnm$ (40 GPa)

All phases, stishovite, *Cmcm*, and anataselike, formed under the simultaneous application of shear stress and hydrostatic pressure in the present studies are previously reported in the constant-pressure simulations with the application of hydrostatic or nonhydrostatic stresses but none of them starting from α-cristobalite has been observed experimentally in silica so far.

We analyze each structure using the KPLOT program to see whether injection of shear components has any influence on the densification mechanism. For all cases considered here, we find the densification mechanism is practically identical and is due to a close-packing anion sublattice, i.e., a slightly distorted hexagonal-close-packed anion sublattice, indicating no effect of the shear stresses on the densification mechanism until the first-order phase transitions occur. On the other hand, the shear stresses play an important role during the first-order phase transformation. One can see from the Table II, introducing shear stress on the *a-b* planes regardless of the other shear-stress components always produce the *Cmcm* phase, signifying that the *a-b* planes are very sensitive to shear deformation. On the other hand, the application of shear stress on the *a-c* planes results in the anataselike structure. Note that in our preliminary work,[13] we also observed the anataselike phase with the application of nonhydrostatic pressure.

In order to understand how these phase transformation proceeds or to expose whether introducing shear stresses yields a different transformation mechanism than the hydrostatic pressure, we next study the pressure dependence of the simulation cell vectors at the transitions pressures. Figure 7 shows the cell lengths and angles as a function of minimization step for the stishovite and anataselike phase. The simulation cell vectors **A**, **B**, and **C** are along the [100], [010],

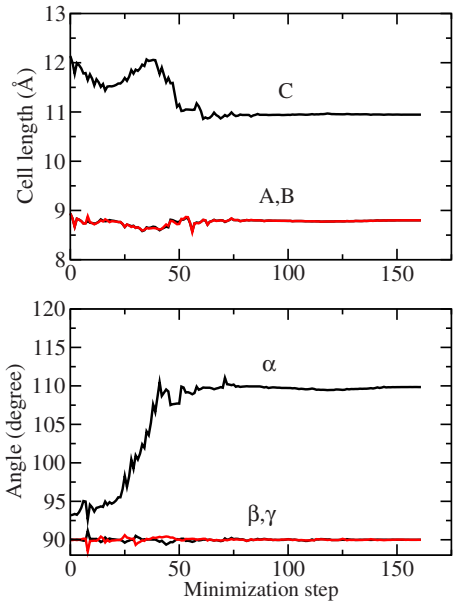

FIG. 8. (Color online) The variation in simulation cell lengths and angles as a function of minimization step during the evolution of the *Cmcm* phase.

and [001] directions, respectively. The magnitude of these vectors is plotted in the figure. The phase transformation into the stishovite phase occurs in two steps: first the cell lengths decouple with two lengths decreasing (along [100] and [010] axes) with a corresponding increase in the third length (along [001] axis). Second the structure is noticeably compressed along the *c* direction while it is expanded slightly along the other directions. On the other hand, the transformation into the anataselike phase proceeds in one step and it is associated with a simultaneous expansion along the *c* direction and a compression along the other directions. In order to form the stishovite structure, the Si atoms make new bonds with O atoms at the adjuncts [001] planes and the SiO_4 tetrahedra rotates while to structure the anataselike state, Si atoms form new bonds with O atoms at the same planes and the transformation does not involve any rotation of SiO_4 tetrahedra. Nevertheless, a careful structural analysis using the KPLOT program suggests that both phase transformations proceed via the same intermediate state having the $P4_12_12$ tetragonal symmetry. The transformation mechanism observed for the stishovite and anataselike phases under the simultaneous application of shear and hydrostatic stresses is similar to what has been observed in the pure hydrostatic pressure (see Ref. 13 for more information and the evolution of the anataselike and stishovite phases).

The phase transformation into the *Cmcm* phase is very straightforward as shown in Fig. 8 and due to the shear deformation on the *a*-*b* planes and a small compression along the *c* axis. This simple deformation produces an orthorhombic intermediate phase within $C222_1$ symmetry before the structure transforms into the *Cmcm* phase. The lattice parameters of $C222_1$ state are $a=5.80$ Å, $b=6.51$ Å, and $c=5.81$ Å at 28 minimization step. The evolution of the *Cmcm* crystal is presented in Fig. 9.

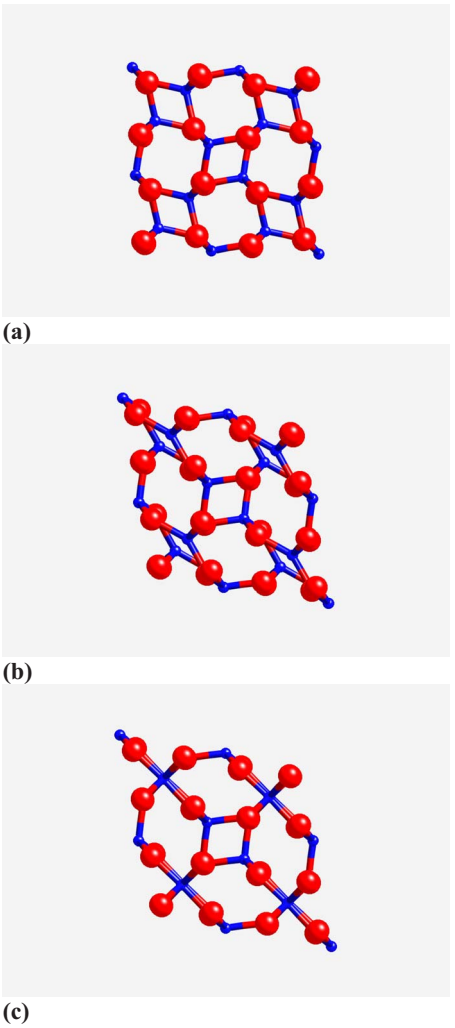

FIG. 9. (Color online) The evolution of the *Cmcm* phase.

IV. CONCLUSIONS

We have studied the behavior of α-cristobalite under pure shear stresses and the simultaneous application of shear stress and hydrostatic pressure using *ab initio* constant-pressure simulations. We find the formation of monoclinic phases having $P2_1$ symmetry when the α-cristobalite is subjected to shear stress on *a*-*c* and *b*-*c* planes. Further increase in shear stress on these planes yields structural failure. On the other hand, α-cristobalite transforms into an orthorhombic phase within $C222_1$ symmetry when it was sheared on the *a*-*b* planes. With further increasing shear stress, the orthorhombic phase converts to a two-dimensional layered monoclinic phase. At zero stress, the layered monoclinic phase transforms into a tetragonal phase ($P\bar{4}m2$), which is also energetically favorable relative to the other phases of silica, observed in the present study. For the simultaneous application of shear stress and hydrostatic pressure, we observe the formation of the *Cmcm*, anataselike, and stishovite structures. The densification mechanism under hydrostatic pressure and the simultaneous application of shear stress and hydrostatic pressure appears to be the same and is associated with a close-packed hexagonal anion sublattice. These

higher-coordinated *Cmcm*, anataselike, and stishovite structures starting from α-cristobalite under pressure have not been observed experimentally yet. However, simulations using different approaches, classical or quantum, suggest the existence of these phases in silica. We should note here that in a contrast to the present and previous *ab initio* simulations[13] in which *Cmcm* and anataselike phases form under nonhydrostatic (shear) stresses, the classical MD simulations[7,8] suggest that these phases can be also form under hydrostatic pressure. The discrepancies between these simulations might be associated with thermal motion or loading conditions. Our simulations were performed at 0 K (relaxation of structure) while the classical MD simulations were performed at finite temperature. Therefore, thermal motion might drive these phase transformations even under hydrostatic pressure.

ACKNOWLEDGMENTS

The visit of the author to Ahi Evran Üniversitesi was facilitated by the Scientific and Technical Research Council of Turkey (TÜBİTAK) BIDEB-2221. The calculations were run on Sacagawea, a 128 processor Beowulf cluster, at the University of Texas at El Paso.

[1] D. C. Palmer and L. W. Finger, Am. Mineral. **79**, 1 (1994).
[2] Y. Tsuchida and T. Yagi, Nature (London) **347**, 267 (1990).
[3] Y. Yahagi, T. Yagi, H. Yakamawaki, and K. Aoki, Solid State Commun. **89**, 945 (1994).
[4] R. J. Hemley, C. T. Prewitt, and K. J. Kingma, Rev. Mineral. **29**, 41 (1994).
[5] L. Huang, M. Durandurdu, and J. Kieffer, Nat. Mater. **5**, 977 (2006).
[6] N. A. Dubrovinskaia, L. S. Dubrovinsyky, S. K. Saxena, F. Tutti, S. Rekhi, and T. Lebihan, Eur. J. Mineral. **13**, 479 (2001).
[7] L. S. Dubrovinsky, N. A. Dubrovinskaia, V. Prakapenka, F. Seifert, F. Langenhorst, V. Dmitriev, H.-P. Weber, and T. Le Bihan, Phys. Earth Planet. Inter. **143-144**, 231 (2004).
[8] M. Yamakata and T. Yagi, Proc. Jpn. Acad., Ser. B: Phys. Biol. Sci. **73**, 85 (1997).
[9] S. Tsuneyuki, Y. Matsui, H. Aoki, and M. Tsukada, Nature (London) **339**, 209 (1989).
[10] Y. Liang, C. R. Miranda, and S. Scandolo, Phys. Rev. Lett. **99**, 215504 (2007).
[11] D. D. Klug, R. Rousseau, K. Uehara, M. Bernasconi, Y. Le Page, and J. S. Tse, Phys. Rev. B **63**, 104106 (2001).
[12] D. Donadio, R. Martoňák, P. Raiteri, and M. Parrinello, Phys. Rev. Lett. **100**, 165502 (2008).
[13] M. Durandurdu, Phys. Rev. B **80**, 024102 (2009).
[14] J. P. Perdew, K. Burke, and M. Ernzerhof, Phys. Rev. Lett. **77**, 3865 (1996).
[15] P. Ordejón, E. Artacho, and J. M. Soler, Phys. Rev. B **53**, R10441 (1996).
[16] N. Troullier and J. L. Martins, Phys. Rev. B **43**, 1993 (1991).
[17] R. Hundt, J. C. Schön, A. Hannemann, and M. Jansen, J. Appl. Crystallogr. **32**, 413 (1999).
[18] M. Zhao, R. Q. Zhang, Y. Xia, and S.-T. Lee, Phys. Rev. B **73**, 195412 (2006).
[19] M. Zhao, Z. H. Zhu, J. D. Gale, Y. Xia, and G. Q. Lu, J. Phys. Chem. C **111**, 9652 (2007).
[20] J. Weissenrieder, S. Kaya, J.-L. Lu, H.-J. Gao, S. Shaikhutdinov, H.-J. Freund, M. Sierka, T. K. Todorova, and J. Sauer, Phys. Rev. Lett. **95**, 076103 (2005).
[21] T. K. Todorova, M. Sierka, J. Sauer, S. Kaya, J. Weissenrieder, J.-L. Lu, H.-J. Gao, S. Shaikhutdinov, and H.-J. Freund, Phys. Rev. B **73**, 165414 (2006).
[22] J. Seifert, D. Blauth, and H. Winter, Phys. Rev. Lett. **103**, 017601 (2009).
[23] S. Kaya, M. Baron, D. Stacchiola, J. Weissenrieder, S. Shaikhutdinov, T. K. Todorova, M. Sierka, J. Sauer, and H.-J. Freund, Surf. Sci. **601**, 4849 (2007).
[24] J.-L. Lu, S. Kaya, J. Weissenrieder, T. K. Todorova, M. Sierka, J. Sauer, H.-J. Gao, S. Shaikhutdinov, and H.-J. Freund, Surf. Sci. **600**, L164 (2006).
[25] In order to compute the EDOS of a single layer, periodic boundary conditions were employed along two directions to create in effect continuous layer while a large vacuum region along the other direction was configured between layers. The layer was related until the maximum force was smaller than 0.02 eV $Å^{-1}$.
[26] Y. N. Xu and W. Y. Ching, Phys. Rev. B **44**, 11048 (1991).
[27] S. Sevik and C. Bulutay, J. Mater. Sci. **42**, 6555 (2007).